Incubation and Photoablation of Poly(methyl methacrylate) at 248 nm. New Insight into the Reaction Mechanism Using Photofragment Translational Spectroscopy

Douglas J. Krajnovich*

IBM Research Division, Almaden Research Center, 650 Harry Road, San Jose, California 95120

Received: June 4, 1996; In Final Form: December 16, 1996[⊗]

The decomposition of poly(methyl methacrylate) (PMMA) under the action of 248 nm, 16 ns laser pulses at 250 mJ/cm^2 was studied in vacuum. A sensitive electron impact ionizer/quadrupole mass spectrometer system was used to measure mass spectra and time-of-flight (TOF) distributions of the neutral photoproducts. The incubation and photoablation reactions were unambiguously resolved in the TOF distributions. The incubation reaction produces slow-moving species with mass peaks at m/e = 15, 28, 29, 30, 31, 32, 59, and 60 which can be assigned to methanol, CO, and methyl formate. These products are consistent with the incubation mechanism proposed by Stuke and co-workers, namely, single-photon absorption at the carbonyl side-chain chromophore followed by side-chain scission. The incubation reaction produces a partially unsaturated and more strongly UV-absorbing polymer backbone. The ablation of this degraded material at 250 mJ/cm^2 produces mainly species with molecular weights < 150 and translational energies around 0.3 eV. The relationship of these results to an extensive and contradictory body of data in the literature is discussed.

Introduction

Despite more than 15 years of work, the mechanism(s) by which organic polymers are ablated or sputtered by pulsed laser radiation are still not well understood. Controversy lingers over the extent to which the material removal process is thermally driven vs electronically or photochemically driven. Nevertheless, a good phenomenological data base has been established on which numerous practical applications have been built.

Two classes of behavior have been identified depending on whether the virgin polymer absorbs strongly or weakly at the laser wavelength. For strongly absorbing polymers, the zeroth-order phenomenological picture is that ablation sets in at a critical threshold fluence and that the ablation rate (depth of material removed per pulse) is independent of pulse number and increases roughly logarithmically with fluence above the threshold fluence. Recent work on polyimide[1] and poly(ethylene terephthalate) (PET)[1,2] challenges this simple picture. For polymers that absorb weakly at the irradiation wavelength, a phenomenon called incubation has sometimes been observed. Incubation is the process whereby a weakly absorbing starting material is converted (through photochemical and/or thermal reactions) into a modified material with a much higher absorption cross section. This degraded material then ablates similarly to a strongly absorbing polymer. If you take an incubating polymer and start irradiating on a virgin spot, the zeroth-order picture is that the ablation rate per pulse starts out near zero and gradually builds to a steady-state value after a few tens or hundreds of laser pulses. The classic example of an incubating polymer is poly(methyl methacrylate) (PMMA) at 248 nm.

Three distinct pictures of PMMA ablation have been presented in the literature. We begin with the work of Stuke and co-workers.[3−5] Larciprete and Stuke[3] irradiated PMMA with 248 nm, 15 ns laser pulses (at an unspecified fluence) and detected neutral products by multiphoton ionization using a 290 nm, 1 ps ionization pulse. Most of the mass peaks detected were between 92 and 160 amu. Production of methyl methacrylate monomer (MMA) at m/e = 100 appeared to be minor. Larciprete and Stuke guessed that most of their signal was due to fragments of an unsaturated backbone following extensive side-chain scission. Küper and Stuke[4] developed this picture further by monitoring UV and IR transmission spectra of thin PMMA films while exposing the films to low-fluence KrF laser pulses or continuous UV light sources. For virgin PMMA, strong UV absorption kicks in around 230−240 nm. With increasing exposure to deep UV light, Küper and Stuke showed that the PMMA undergoes a steep increase in absorption over a wide range of wavelengths, extending all the way to the visible. The increase in UV absorption is accompanied by new bands in the IR spectrum, including bands indicative of C=C bonds, a band characteristic of triple or conjugated double bonds, a new ester band, and a band characteristic of free −OH groups. They interpreted these results in terms of one-photon absorption at the carbonyl side-chain chromophores, followed by photodecomposition to produce an unsaturated polymer backbone and side-chain fragments. The partially conjugated polymer backbone is responsible for the red-shifted and strengthened UV absorption which then allows photoablation of the backbone to occur at either 248 or 308 nm. In effect, the PMMA dopes itself with strongly absorbing unsaturated compounds.

This viewpoint was refined in a follow-up study by Küper, Modaressi, and Stuke[5] (hereafter referred to as KMS). KMS synthesized the following model compound and studied its photochemistry in hexane solution:

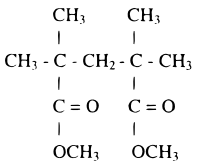

They observed a well-defined photochemical fragmentation pattern indicating that side-chain scission is in fact the dominant primary process, accompanied by formation of a C=C bond in the main chain. KMS suggest that the side chain fragment, $^{\bullet}COOCH_3$, either extracts a hydrogen from the backbone (or the solvent) to form methyl formate, or decomposes to give

* Author to whom correspondence should be addressed. Current address: Western Digital Corporation, 2109 Tasman Drive, Santa Clara, CA 95054.

⊗ Abstract published in *Advance ACS Abstracts,* March 1, 1997.

S1089-5639(96)01620-9 CCC: $14.00

$CO_2 + CH_4$ and/or $CO + CH_3OH$. KMS directly detected methyl formate and CH_3OH in their solution experiment but they were not equipped to detect the presence of CO_2 or CH_4. Additional support for side-chain scission comes from an early mass spectrometric study by Estler and Nogar.[6] These authors irradiated PMMA in vacuum using low-fluence 266 and 240 nm laser pulses. At 240 nm, in particular, they found methyl formate to be a major photoproduct.

The second picture of PMMA ablation comes from studies by Tsunekawa et al.[7] and Blanchet and Fincher.[8] Tsunekawa et al. irradiated PMMA in vacuum with 308 nm laser pulses and detected neutral products by multiphoton ionization using 248 nm or 193 nm laser pulses. Their mass spectrum looks quite different from that of Larciprete and Stuke. Their strongest peaks lie between $m/e = 41$ and 169, with significant signal at the MMA parent mass ($m/e = 100$). They conclude that most of the signal is due to MMA monomers and dimers and argue that PMMA decomposes by a thermal "unzipping" reaction. Blanchet and Fincher irradiated PMMA with 266 nm, 10 ns laser pulses at fluences between 0.1 and 1 J/cm^2 and detected neutral photoproducts with a quadrupole mass spectrometer. They also measured mass spectra during steady-state pyrolysis of a PMMA sample, where the reaction in known to proceed by unzipping. They observed a close correspondence between the two mass spectra and concluded that the mechanism involves unzipping in both cases. The two studies mentioned in this paragraph did not explicitly address the issue of incubation.

A third picture of PMMA ablation comes from a series of studies by Srinivasan and co-workers.[9−11] PMMA photoproducts were analyzed indirectly by Srinivasan et al.,[9] who irradiated PMMA samples in a glass vacuum cell and collected the volatile products in a liquid nitrogen trap. The products were analyzed by gas chromatography/mass spectroscopy (GCMS). For 248 nm irradiation at an unspecified fluence, they claim that the majority of the trapped material consists of oligomers of PMMA with 25−40 monomer units. Small amounts of CO_2 and MMA were detected in the trap, but no methanol or methyl formate. For 193 nm irradiation a larger proportion of MMA was detected, but still no methanol or methyl formate. In the same study,[9] Srinivasan et al. report direct laser-induced fluorescence (LIF) detection of C_2 molecules with translational energies as high as 6 eV. They suggest that ablation involves a photochemical breakup of the polymer chain into oligomers along with production of gases such as C_2, CO_2, CO, and MMA. The light gases, in turn, escape from the surface with high velocities, carrying solid particles of the polymer along. Dyer and Srinivasan[10] used a pyroelectric detector to measure time-of-flight distributions of PMMA ablation products in vacuum during 248 nm exposures at fluences between 450 and 570 mJ/cm^2. They observed a weak peak with an average velocity of 1.6×10^5 cm/s and a strong peak with an average velocity of 2×10^4 cm/s. The products were not mass resolved. Dyer and Srinivasan assumed that the fast peak must be due to small fragments such as C_2, CO, and CO_2 and that the slow peak was due to the oligomers observed in the previous study.

Srinivasan, Braren, and Casey (SBC)[11] published another study in which they investigated the nature of the incubation phenomenon. For 248 nm irradiation at 0.9 J/cm^2, they observed a slight bulging of the surface up to 15 pulses or so due to chemical transformation of the material. This partially decomposed material could be washed out by an unspecified solvent. After about 40 pulses a steady-state ablation rate was established, with the formation of an etch crater and a reduced solvent effect. SBC attribute incubation to "insufficient production of the gaseous products that are needed to build up sufficient pressure to eject large fragments into which the solid is largely broken up". They are skeptical that the incubation mechanism proposed by KMS applies under true ablation conditions. They argue that their failure to detect significant amounts of MMA, methyl formate, or methanol rules out both a simple unzipping reaction and a dominant role of the KMS incubation reaction. Additional discussion of the mechanism has been given by Srinivasan.[12]

The present work was motivated primarily by the KMS study. The goal was to see if the incubation and ablation reactions could be separately discerned in the mass and translational energy distributions of the neutral photofragments. In the field of chemical reaction dynamics, the technique of using translational energy distributions to infer the dynamics of gas-phase photochemical reactions is often referred to as photofragment translational spectoscopy. We show here that photofragment translational spectroscopy can also yield insights into a rather complicated solid-state decomposition reaction. We state in advance that our results are in excellent agreement with the KMS incubation picture.

Experimental Details

The apparatus on which these experiments were performed is described in detail in ref 13. Briefly, it consists of a large sample chamber with a rotatable/translatable sample holder and a differentially-pumped quadrupole mass spectrometer with a liquid nitrogen cooled electron impact ionizer and an off-axis scintillation-type particle counter. The electron energy was set at 20 eV to minimize fragmentation during ionization. During the experiments, the sample chamber pressure was around 10^{-6} Torr while the ionization chamber pressure was below 10^{-10} Torr.

The sample was cut from a 3.2 mm thick sheet of high-purity PMMA containing no additives or stabilizers (Rohm GS 214). The irradiation source was a Lumonics KrF excimer laser (248 nm) with a fwhm pulsewidth of 16 ns. The laser beam was focused into a solid CaF_2 light tunnel rod, and the output face of the light tunnel was reimaged onto the sample. The beam profile at the image plane was almost top hat in both the *X* and *Y* directions (see Figure 2 of ref 13). For all of the experiments reported here, the angle of incidence was 45°. At this angle the detector samples species emitted along the surface normal. Mass spectra and time-of-flight distributions of the neutral photofragments were obtained by gating or multiscaling the mass spectrometer output using single-ion-counting electronics. For measurements of the high-mass tail of the product distribution, the quadrupole was operated with the pole dc voltage OFF. In this mode of operation, the quadrupole serves as a high-pass filter, efficiently transmitting all ions with *m*/*e* values greater than a cutoff value determined by the radio frequency (rf) voltage setting.

Results and Analysis

In ref 14, Küper and Stuke report that the PMMA ablation threshold for 16 ns, 248 nm laser pulses is around 500 mJ/cm^2. The lowest etch rate plotted in ref 14 is ∼1000 Å/pulse, which is still quite high. Due to the high sensitivity of our mass spectrometer, we were able to go lower in fluence. All of the measurements reported here were done at an incident fluence of 250 mJ/cm^2. The steady-state etch rate at this fluence was measured to be 300 ± 50 Å/pulse using stylus profilometry.

Unlike polyimide and PET,[1,2] which experience a rapid falloff in etch rate per pulse at near-threshold fluences due to radiation hardening, the PMMA etch rate holds steady for thousands of pulses after the initial incubation period. This makes mass scans and TOF measurements easy since one can stay on the same

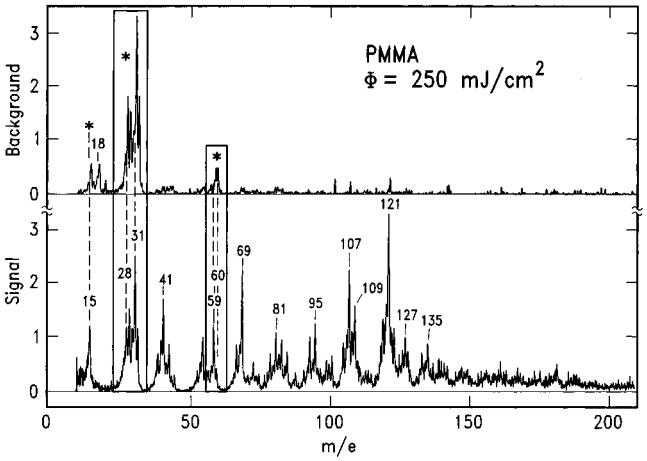

Figure 1. Mass spectrum of PMMA photoproducts under steady-state ablation conditions at 250 mJ/cm^2. The background gate was set to 80−84 ms after each laser pulse and the (signal + background) gate was set to 0−4 ms with the laser running at 10 Hz. The bottom spectrum represents the difference of the (signal + background) and background spectra.

sample spot for considerable lengths of time without worrying about the signals changing.

A mass spectrum taken under steady-state ablation conditions is shown in Figure 1. Since the quadrupole can only pass one mass-to-charge (*m*/*e*) value on each laser pulse, this spectrum was obtained by stepping the quadrupole over the entire mass range and averaging over a certain number of laser pulses at each *m*/*e* value. The entire mass scan took 8000 pulses. Actually, two spectra were acquired simultaneously, corresponding to two different gate intervals following each laser pulse. A signal plus background spectrum was acquired using a gate interval of 0−4 ms. This is wide enough to encompass the usual laser-correlated time-of-flight signal. At the same time, a background spectrum was acquired using a gate interval of 80−84 ms. The laser pulse rate was 10 Hz. The top trace in Figure 1 is the background, while the bottom trace is the difference between the signal plus background and background spectra.

For any normal laser ablation system, if the background gate is set so long after the laser pulse, one would detect only the intrinsic (steady-state) detector background, i.e., there would be a moderately strong background peak at *m*/*e* = 28 and much weaker peaks at *m*/*e* = 12, 14, 15, 16, 17, 18, and 44. These are the usual ultrahigh vacuum background peaks due to CO, CH_4, CO_2, and H_2O. The background mass spectrum in Figure 1 is completely different. In fact, most of the intensity in this "background" spectrum is coming from the PMMA sample! (The intrinsic background with the detector closed is much weaker and occurs only at the UHV masses mentioned above). As we shall see, the large background intensity in the three regions marked by asterisks in Figure 1 is a telltale sign of the incubation reaction.

Figure 2 gives a better view of the *m*/*e* = 25−35 region. The top panel of this figure shows the intrinsic background with the detector closed. The middle panel shows the background recorded in the 80−84 ms gate interval with the detector open to the PMMA sample and the laser pulsing at 10 Hz. The bottom panel shows the laser-correlated signal in the 0−4 ms gate interval after subtracting background.

The conclusion from this is that PMMA is emitting a quasi-steady-state background flux of material which gives mass peaks at *m*/*e* = 28, 29, 30, 31, and 32, and also *m*/*e* = 15, 59, and 60. Of course, if the laser pulse rate is reduced sufficiently, this

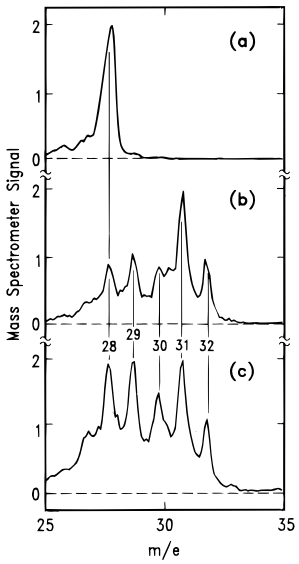

Figure 2. Expanded view of the *m*/*e* = 25−35 region: (a) background spectrum with the detector closed; (b) background spectrum with the laser pulsing on PMMA; (c) signal spectrum with laser pulsing on PMMA. Gate intervals same as in Figure 1. Note that, for easy comparison, all 3 panels have been scaled to the same peak height. The actual signal level was much lower in (a) than in (b) and in (b) than in (c).

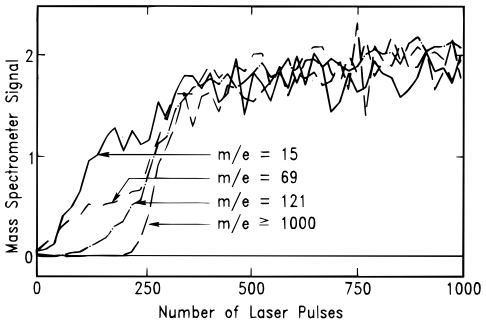

Figure 3. Laser-correlated mass spectrometer signal at four different masses as a function of the cumulative number of laser pulses on a fresh spot. After 300−500 laser pulses, the incubation and ablation reactions have reached steady-state and the relative yields of different mass species becomes constant.

"background" signal must decay to zero between laser pulses; evidently a 10 Hz pulse rate is fast enough to maintain a quasi-steady signal. The fact that there is no quasi-steady signal above *m*/*e* = 60 suggests that this signal is due to the side-chain scission reaction. According to the mass spectral tables,[15] both methanol and methyl formate yield strong peaks at *m*/*e* = 29, 31, and 32. Methyl formate, in addition, is expected to give a strong parent peak at *m*/*e* = 60, whereas we see weak peaks at both *m*/*e* = 59 and 60. The mass 59 peak may be due to $^{\bullet}COOCH_3$ radicals that escape from the sample without abstracting a hydrogen atom. The *m*/*e* = 28 peak can be accounted for by CO molecules from the CH_3OH + CO decomposition channel. The absence of peaks at *m*/*e* = 16 and 44 suggests that the CH_4 + CO_2 decomposition channel is unimportant. (Both CH_4 and CO_2 mainly produce parent ions on electron impact ionization.) It is more difficult to explain the relatively strong peaks observed at *m*/*e* = 15 and 30. Neither methanol nor methyl formate is expected to yield much intensity at these masses.[15] These peaks can be rationalized if $^{\bullet}CH_3$ and $^{\bullet}CH_2OH$ radicals are also byproducts of the side-chain scission reaction.

Figure 3 shows the growth of the laser-correlated signal at several different masses as a function of the cumulative number

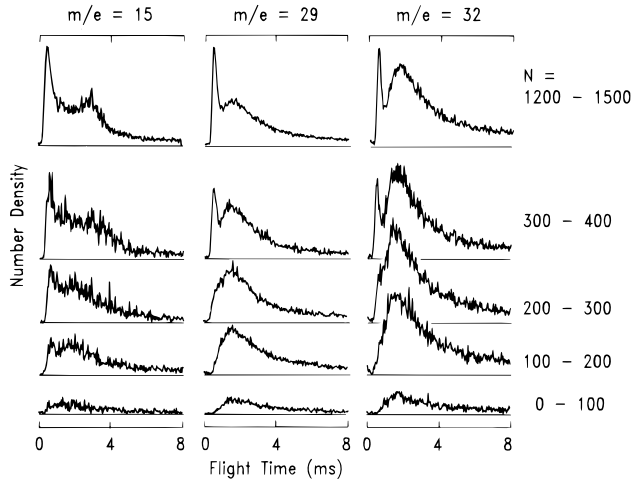

Figure 4. Time-of-flight spectra of products detected at $m/e = 15$, 29, and 32 as a function of the cumulative number of laser pulses N on a fresh spot. The slow peak is due to the methyl formate and methanol products of the incubation reaction, while the fast peak which grows in later is due to the ablation of degraded polymer material.

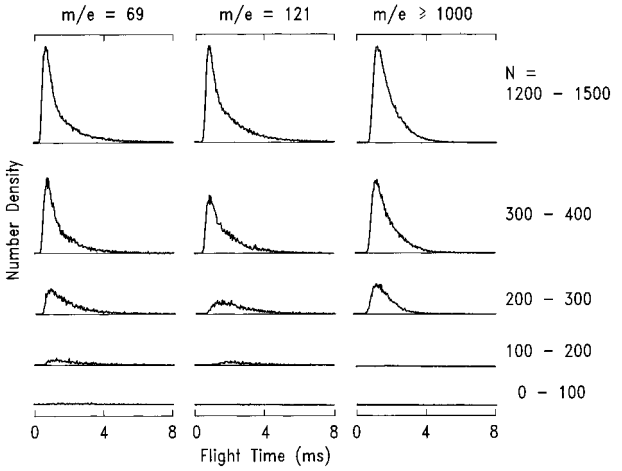

Figure 5. Same as Figure 4, except for products detected at $m/e = 69$, $m/e = 121$, and $m/e \geq 1000$. At these masses, there is no contribution from the incubation reaction. Only a fast peak is observed which grows in late.

of laser pulses. A fresh target spot was used at each m/e value. The signal increases most rapidly at $m/e = 15$, since this mass samples the incubation reaction products directly. At higher m/e values there is a longer incubation time before the signal starts to grow. After 300−500 pulses, the signals at all m/e values have reached steady-state and lead to a mass spectrum similar to Figure 1.

The distinction between incubation and ablation reactions is even more striking in the time-of-flight (TOF) distributions. Figure 4 shows TOF distributions at three m/e values that sample the incubation reaction. The TOF distributions are plotted on an absolute intensity scale as a function of the cumulative number of laser pulses, N. In the first 100 pulses, only a weak, slow TOF signal is observed. As N increases, the slow peak grows in intensity and a fast TOF peak appears. After 500 pulses or so, there is no further change in the ratio of the fast and slow TOF components. In my opinion, the slow TOF peak is due to the products of the side-chain scission reaction, while the fast peak is due to photoablation of the unsaturated polymer backbone. If this explanation is correct, then we should see only the fast TOF peak at all masses greater than 60 amu. This is in fact the case. Figure 5 gives several examples. Note the delayed onset of the fast ablation signal and the complete absence of the slow TOF signal at these masses.

The TOF number density distributions, $N(t)$, may be inverted to translational energy flux distributions, $P(E)$s, if we can assign the mass of the neutral species that gives rise to the ionizer signal at each m/e value. The inversion uses the known flight distance from the PMMA target to the ionizer (69.2 cm), and a small correction to the measured flight times to account for the ion flight time through the quadrupole. Figure 6 shows examples of the $P(E)$'s obtained from the $m/e = 29$ TOF distributions. There is little doubt that the slow TOF peak is due to CH_3OH, so we assume a neutral mass of 32 for the inversion. The fast TOF peak may include contributions from many neutral species with masses greater than or equal to 29. For lack of better information, we assume a neutral mass of 32 for the fast peak as well. (This will give a lower bound to the fast peak translational energy distribution.)

In the top panel of Figure 6, corresponding to $N = 100-200$, we see only a low-energy peak in the translational energy flux distribution. As the inset shows, the energy distribution is well-approximated by an exponential with a mean energy of 0.033 eV. (Recall that at room temperature, $kT = 0.025$ eV.)

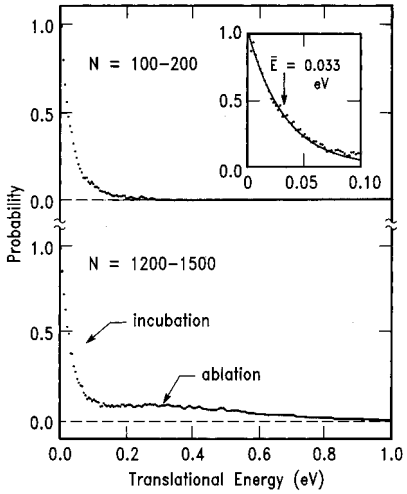

Figure 6. Translational energy flux or probability distributions obtained by inverting the $m/e = 29$ TOF spectra. The TOP panel corresponds to the early incubation stage (first 100 pulses). The dots represent a direct inversion of the experimental TOF distribution, assuming that the $m/e = 29$ signal is exclusively due to methanol (neutral mass = 32). The solid curve in the inset is an exponential fit with a mean translational energy of 0.033 eV. If instead the $m/e = 29$ signal is largely due to methyl formate (neutral mass = 60), the energy scale would be increased by a factor of 2. The bottom panel corresponds to the steady-state etching regime where incubation and ablation reactions proceed in parallel.

This low energy, combined with the quasi-steady-state nature of the flux, suggests that the incubation products are slowly effusing out from deep within the PMMA target. In the bottom panel of Figure 6, corresponding to $N = 1200-1500$, we still see the low-energy incubation component but there is also a high-energy component due to photoablation. The ablation component has a mean energy of a few tenths of an eV with a tail extending out to about 1 eV.

Figure 7 shows $P(E)$'s obtained at six masses that are not contaminated by the incubation reaction. Again we assume that the dominant contributing neutral mass at each m/e value is the same as the detected ion mass. This assumption is certainly violated to some extent, but at least it has the advantage that the derived energies are a rigorous lower bound to the true energies. (For example, if the signal at $m/e = 41$ originates mainly from neutrals with $m = 80$, the energy scale would be stretched by a factor of two.) The main point of Figure 7 is that the mean translational energy of the ablation fragments is around

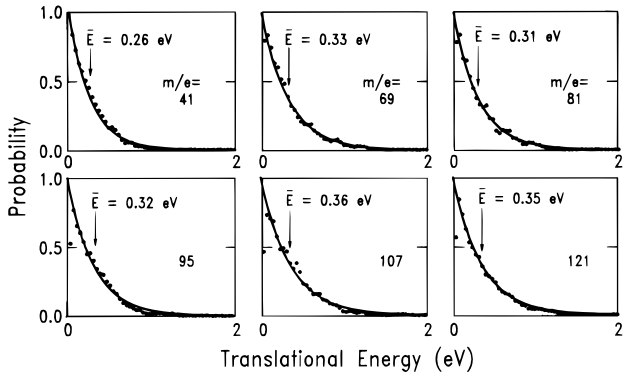

Figure 7. Translational energy distributions obtained under steady-state etching conditions for six of the prominent mass peaks in Figure 1. At these mass peaks, there is no contribution from the incubation reaction. The dots correspond to a direct inversion of the experimental TOF distributions, under the assumption that the neutral mass equals the ion mass in each case. (If cracking of larger species occurs in the ionizer the energies would of course be higher.) The solid curves are best-fit exponentials with the mean energies indicated by the arrows.

0.3 eV and is not strongly dependent on fragment mass over a factor of three mass range.

The direct mass spectrometric studies also prove that the energetic C_2 species observed by Srinivasan et al.[9] constitutes a negligibly small fraction of the total ablation flux, i.e., no mass peak is observed at $m/e = 24$ in Figure 1 even though it is known[13] that C_2 gives mainly parent ion under electron impact ionization. The only reason they can detect C_2 is because of the extraordinarily high sensitivity and selectivity of laser-induced fluorescence. In our opinion, C_2 is produced in such tiny amounts that it cannot be used to infer anything about the average progression of the ablation reaction. Similarly, the absence of a strong peak at $m/e = 44$ indicates that CO_2 is not a major incubation or ablation product.

A few additional comments should be made concerning the high-mass tail of the product distribution since this bears upon the question of whether a major fraction of the ablated mass might be ascribed to high molecular weight oligomeric species. Above $m/e = 200$, the signal level at any single product mass was far too low to generate any meaningful data. This does not prove that high-mass species are negligible. To get a better handle on this, we operated the quadrupole as a high-pass filter by turning the pole dc voltage OFF. The rf voltage was varied to give different high-pass cutoff values. For example, with the quadrupole set to transmit all ions with $m/e \geq 200$, we measured an integrated signal level of 2080 (in normalized ion counts). When the cutoff value was increased to 500 amu, the normalized signal dropped to 560, and when the cutoff value was increased to 1000 amu, the normalized signal dropped to 100. This indicates that, in terms of normalized ion counts, there is $(2080 - 560)/100 = 15$ times more signal between 200 and 500 amu than there is at masses greater than 1000 amu. It was difficult to make measurements in high-pass mode with cutoff values less than 200 amu because the signal level increased too rapidly and caused detector saturation even at extremely low electron emission currents. Therefore, we are confident that *in terms of raw ion counts*, the ablation signal is strongly peaked at low m/e values, and in a coarse-averaging sense, the signal decreases rapidly with increasing mass.

Of course, one ion count at 1000 amu corresponds to 10 times more ablated material (on a mass basis) than one ion count at 100 amu. However, the ionization cross section (and hence the detection probability) is also larger for higher mass species. A common rule-of-thumb is that the electron impact ionization cross section is proportional to the molecular polarizability or to the square root of the molecular polarizability. The polarizability, in turn, is a measure of the volume of the electronic charge distribution and is therefore proportional to the size and mass of the neutral species. The higher ionization probability of high-mass species partially offsets the fact that they carry more mass. While there is considerable leeway in these arguments, the conclusion that low molecular weight species dominate under our experimental conditions is likely to be valid, at least in a qualitative sense.

Discussion

In the Introduction we discussed three pictures that have been offered for how PMMA decomposes under pulsed UV laser irradiation. In the first picture, advocated by Stuke and co-workers,[3−5] PMMA undergoes single-photon absorption at the carbonyl chromophore followed by side-chain scission, which results in the formation of side chain fragments and a highly defective, unsaturated backbone which then absorbs strongly and undergoes photoablation. In the second picture, advocated by Tsunekawa et al.[7] and Blanchet and Fincher,[8] PMMA decomposes mainly by thermal unzipping, producing lots of monomer and perhaps also dimer MMA. Incubation in this case involves photochemical creation of chain breaks or initiation sites from which the unzipping reaction can proceed. (There is consensus in the literature that thermal initiation is too slow to explain the experimental results.) The third picture, advocated by Srinivasan and co-workers,[9−12] is that the incubation pulses break up the polymer into large chunks but do not create the same fraction of gaseous products as pulses following the incubation. When the production of gaseous products becomes sufficiently high, they argue, these products generate an explosive force which propels oligomeric fragments out of the ablated volume. Dyer and Srinivasan[10] speculate that stepwise excitation at a small number of absorbing sites in the polymer produces the requisite number of small fragments with high translational energies to cause ablation.

The results presented in this paper strongly support the picture of incubation proposed by Küper and Stuke.[4] We have detected the production of slow neutral species during the incubation period with mass spectrometer peaks at $m/e = 15$, 28, 29, 30, 31, 32, 59, and 60. This is exactly what one would expect for the production of methanol, carbon monoxide, and methyl formate. Not only is there a slow burst of these species following each laser pulse, but these species continue to effuse out of the sample for times in excess of 100 ms, the time between laser pulses. This is why we see excessive "background" at these mass peaks during the mass scan. The fact that incubation products continue to effuse out of the sample for long times after each laser pulse suggests that the incubation reaction is occurring fairly deep within the sample, not only during the incubation interval but also during steady-state ablation. Srinivasan[11] has objected to the incubation mechanism put forward by Stuke and co-workers on the grounds that their studies were performed at such low fluences that their results may not be applicable to true ablation conditions. Our study was performed at a fluence five to six times higher than that used by Küper and Stuke[4] and is sufficient to cause sustained ablation at a rate of 300 Å/pulse. An example of a smooth etch crater formed after 2000 laser pulses at 250 mJ/cm^2 is shown in Figure 8. Millimeter-deep craters have been made by continued pulsing at this fluence. If this is not "true ablation", then better definitions are called for.

After reaching steady-state ablation conditions, the TOF spectra of mass peaks like $m/e = 15$, 29, and 32 contain slow contributions from the incubation products as well as fast

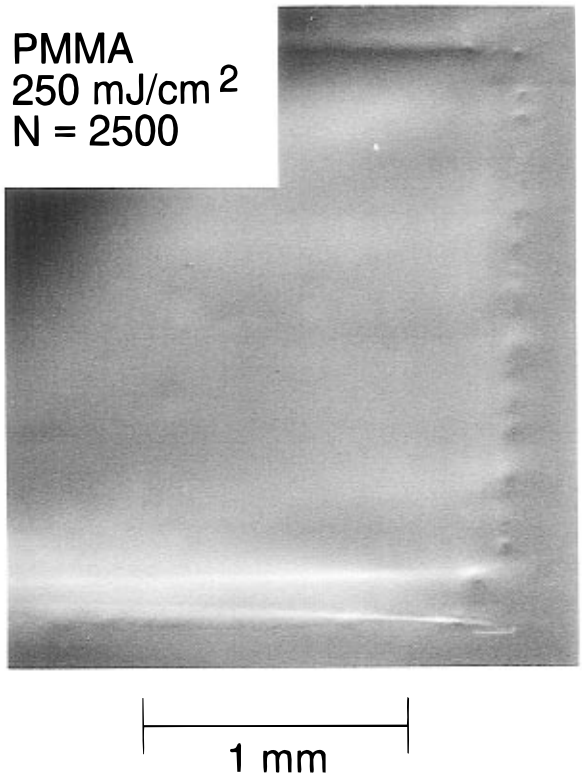

Figure 8. Scanning electron microscope photograph of a PMMA spot exposed for 2500 pulses at 250 mJ/cm^2. Parts of the top, bottom, and right edges of the rectangular illumination spot are visible. The etch pocket is smooth and showed no obvious signs of bubbling or disruption even at much higher magnifications. Evidently PMMA is quite permeable to the incubation gases which effuse out of the sample.

contributions from ablation products which ionize to give fragments at those masses. At masses greater than $m/e = 60$, without exception, only the fast ablation peak is observed. It is of interest to compare our electron impact ionization mass spectrum (bottom panel, Figure 1) to the one shown in Figure 2 of the paper by Blanchet and Fincher.[8] The latter authors omit several details, such as the electron energy, the number of pulses delivered to the sample before and during the measurement, and the particular fluence used to generate their Figure 2. (From their Figure 3, it is clear that their measurements spanned the range 100−1000 mJ/cm^2 which overlaps our work.) Blanchet and Fincher observed strong signals at $m/e = 41$, 69, and 100, as well as a fairly strong cluster of unresolved peaks around $m/e = 30$. We also observe strong peaks at $m/e = 41$ and 69 and of course in the $m/e \approx 30$ region, but we observe only a weak peak at $m/e = 100$. In addition we see other strong peaks both above and below the monomer MMA parent mass ($m = 100$). There is a weak tail of intensity extending up to and beyond $m/e = 1000$, but the intensity falls off quickly with increasing mass. While Blanchet and Fincher argued from their mass spectrum that mainly monomer MMA is produced, our mass spectrum suggests a more complicated mix of fast ablation products, including some intact monomer MMA but also fragments from dimers and fragments of the partially unsaturated polymer backbone created by the incubation reaction. Neither of these in situ mass spectrometric studies supports the claim of Srinivasan et al. that the majority of the PMMA ablation flux consists of MMA oligomers in the 2500−4000 amu range. However, if Srinivasan et al. used much higher fluences for their product collection studies (the actual fluence was not specified in their papers), then perhaps the results are not mutually inconsistent.

Perhaps the most interesting comparison is between our results and the bimodal TOF distribution of PMMA ablation products observed by Dyer and Srinivasan[10] using a pyroelectric detector. In particular, compare Figure 2c of ref 10 with Figure 4 of the present paper. As mentioned in the Introduction, Dyer and Srinivasan argued that the fast peak was due to low molecular weight species like C_2, CO, and CO_2, and that the slow peak was due to heavy oligomeric fragments. They used this to justify the explosive decomposition picture. The results of the present paper suggest an obvious reinterpretation of Dyer and Srinivasan's data: namely, their slow peak is actually due to condensible incubation products (methyl formate and methanol) while their fast peak is due to all products of the ablation reaction, not just light species. Again, since the fluence range for these experiments differs by a factor of two and the ablation rate differs by about a factor of three, one could play devil's advocate and argue that the mechanism completely flip-flops between 250 and 500 mJ/cm^2, i.e., at 250 mJ/cm^2, the fast peak is due to heavy ablation products and the slow peak is due to light incubation products, while at 500 mJ/cm^2, the fast peak is due to light incubation products and the slow peak is due to heavy ablation products. We consider this extremely unlikely, but additional studies bridging the 250−500 mJ/cm^2 fluence gap are needed to prove this to everyone's satisfaction. Sample purity is another variable that could conceivably affect comparisons between labs. The PMMA samples used here were specially prepared high-purity bulk samples of the same type used by Küper and Stuke. The purity of the PMMA used by Dyer and Srinivasan was not specified.

Conclusions

The results of the present experiments at 250 mJ/cm^2 are entirely consistent with the incubation mechanism proposed by Stuke and co-workers. According to this picture, incubation is a manifestly photochemical reaction involving single-photon absorption at the carbonyl side-chain chromophore followed by side-chain scission to produce methanol, CO, and methyl formate. The fate of the degraded material left behind by the incubation reaction is less certain. According to the present study, PMMA that is incubated at 250 mJ/cm^2 ablates to give mainly low molecular weight fragments ($m < 150$) with mean translational energies around 0.3 eV. These translational energies are lower than observed in polyimide and poly(ethylene terephthalate) at comparable 248 nm ablation rates but are still probably higher than $2kT_s$, where T_s is the peak surface temperature. It is reasonable to expect some degree of thermal unzipping in the incubated material, since, as KMS[5] showed, the incubation reaction introduces some main chain breaks (even though side chain breaks predominate). The smaller number of main chain breaks can serve as initiation sites for thermal unzipping. An important difference is that the material being unzipped is degraded and has some fraction of side chains missing and some fraction of C═C bonds. The unzipping reaction will almost certainly stop if it encounters a C═C bond.

Acknowledgment. We thank Dr. Stefan Küper for the high-purity PMMA sample and other helpful information.

References and Notes

(1) Krajnovich, D. J.; Vazquez, J. E. *J. Appl. Phys.* **1993**, *73*, 3001.
(2) Krajnovich, D. J., submitted for publication.
(3) Larciprete, R.; Stuke, M. *Appl. Phys. B* **1987**, *42*, 181.
(4) Küper, S.; Stuke, M. *Appl. Phys. A* **1989**, *49*, 211.
(5) Küper, S.; Modaressi, S.; Stuke, M. *J. Phys. Chem.* **1990**, *94*, 7514.

(6) Estler, R. C.; Nogar, N. S. *Appl. Phys. Lett.* **1986**, *49*, 1175.
(7) Tsunekawa, M.; Nishio, S.; Sato, H. *J. Appl. Phys.* **1994**, *76*, 5598.
(8) Blanchet, G. B.; Fincher, C. R., Jr. *Appl. Phys. Lett.* **1994**, *65*, 1311.
(9) Srinivasan, R.; Braren, B.; Seeger, D. E.; Dreyfus, R. W. *Macromolecules* **1986**, *19*, 916. Srinivasan, R.; Braren, B.; Dreyfus, R. W.; Hadel, L.; Seeger, D. E. *J. Opt. Soc. Am. B* **1986**, *3*, 785. (These two articles are almost identical.)
(10) Dyer, P. E.; Srinivasan, R. *J. Appl. Phys.* **1989**, *66*, 2608.
(11) Srinivasan, R.; Braren, B.; Casey, K. G. *J. Appl. Phys.* **1990**, *68*, 1842.
(12) Srinivasan, R. *J. Appl. Phys.* **1993**, *73*, 2743. (See especially pp 2748−9 of this article.)
(13) Krajnovich, D. J. *J. Chem. Phys.* **1995**, *102*, 726.
(14) Küper, S.; Stuke, M. *Appl. Phys. B* **1987**, *44*, 199.
(15) Stenhagen, E.; Abrahamsson, S.; McLafferty, F. W. Registry of Mass Spectral Data; Wiley: New York, 1974.